21St Century Atmospheric Forecasting for Space Based Applications

Randall J. Alliss, Billy D. Felton, Mary Ellen Craddock, Heather Kiley, Michael Mason

Northrop Grumman Mission Systems
7555 Colshire Dr
McLean, VA 22102

Abstract

Many space based applications from imaging to communications are impacted by the atmosphere. Atmospheric impacts such as optical turbulence and clouds are the main drivers for these types of systems. For example, in space based optical communications, clouds will produce channel fades on the order of many hundreds of decibels (dB) thereby breaking the communication link. Optical turbulence can also produce fades but these can be compensated for by adaptive optics.

The ability to forecast the current and future location and optical thickness of clouds for space to ground Electro Optical or optical communications is therefore critical in order to achieve a highly reliable system. We have developed an innovative method for producing such forecasts. These forecasts are intended to provide lead times on the order of several hours to days so that communication links can be transferred from a currently cloudy ground location to another more desirable ground site. The system uses high resolution Numerical Weather Prediction (NWP) along with a variational data assimilation (DA) scheme to improve the initial conditions and forecasts. DA is used to provide an improved estimate of the atmospheric state by combining meteorological observations with NWP products and their respective error statistics. Variational DA accomplishes this through the minimization of a prescribed cost function, whereby differences between the observations and analysis are damped according to their perceived error. The NWP model is a fully three-dimensional (3D) physics-based model of the atmosphere initialized with gridded atmospheric data obtained from a global scale model. The global model input data has a horizontal resolution of approximately 25km, which is insufficient for the desired atmospheric forecasts required at near 1km resolution. Therefore, a variational DA system is used to improve the quality and resolution of the initial conditions first prescribed by the global model. Data used by the DA system are local surface observations of temperature, pressure, winds and moisture (also known as the Standard Meteorological Variables, SMV), local vertical soundings of SMV, and local radar reflectivities from the National Weather Service NEXRAD radar network.

A series of DA experiments have been set up and conducted on the Maui High Performance Computing System, Riptide supercomputer. Initial results show a marked improvement of the cloud and optical turbulence forecasts over the control run without data assimilation. Detailed results will be presented at the conference.

1. INTRODUCTION

Space to ground bandwidth requirements have steadily increased over the last five decades as the sophistication of Earth observing and intelligence gathering has greatly improved. However, the Radio Frequency (RF) spectrum over which this data is transmitted may be reaching a tipping point. RF signals have been relied on exclusively to communicate with spacecraft since satellite communications began, but there are increasing challenges that may prevent RF communications from fully meeting current and future requirements. These technology and regulatory limitations may be alleviated, in part, by Free-Space Optical Communications (FSOC) systems. There are several key advantages to using FSOC to perform space based communications. Data can be transmitted through free-space via lasers at very high data rates at multi-Gb/s over long distances. Optical beams are very narrow, and are much less susceptible to interference than RF signals. Unlike RF, the optical spectrum is currently unregulated. Finally, optical communications systems are relatively small in size, weight, and power (SWAP) and potentially much less expensive than comparable RF systems, particularly for space to ground missions.

The ultimate realization of practical, high-availability FSOC systems, however, will depend upon how well they mitigate the impacts of atmospheric effects, primarily cloud cover and optical turbulence (OT). Clouds are the largest source of atmospheric attenuation for space-to-ground optical communications, often producing transmission losses of several decibels (dB) to several tens of dB. Without impractically large link margins (>>3dB), most clouds are generally considered blockages to FSOC links. Optical turbulence distorts light as it travels through the atmosphere, creating fluctuations in the power received by the ground station and distortions of the phase of the transmitted wave. Though usually not as significant a problem as clouds and turbulence, aerosols also attenuate optical signals and must be accounted for in a system's link budget. Finally, operations of FSOC systems can be affected by standard weather conditions; in particular, high winds, precipitation, and condensation may force closure of an open dome to protect sensitive optical equipment. Each of these atmospheric effects requires one or more different mitigation strategies, which may in turn be dependent on the operational design of a particular system.

The objective of this work is to develop and mature a state of the art atmospheric modeling system that generates high resolution forecasts of clouds, OT, surface temperature, humidity and winds in order to feed a decision aid system for link handover between multiple, geographically diverse FSOC ground sites. Section 2 describes the technical approach in developing the modeling system. Section 3 shows examples from the model output and Section 4 shows model results and validation.

2. TECHNICAL APPROACH

In past studies, we have used Numerical Weather Prediction (NWP) modeling to quantify the effects of the atmosphere on FSOC communications [1]. The NWP model was used to develop a climatology of OT over the summit of Haleakala on the island of Maui. In addition, the model was used to generate a three-dimensional representation of C_n^2 and other atmospheric parameters in both the planetary boundary layer and the free atmosphere that identified and forecast cloud blockages and poor seeing conditions. In this study, we use a new and improved version of this model which is described below.

a. WRF Model Setup

In this study we use version 3.6.1 of the Weather Research and Forecasting (WRF) model developed jointly by the National Center for Atmospheric Research (NCAR) and the National Oceanic and Atmospheric Administration (NOAA) [2]. WRF is a mesoscale NWP model developed for the prediction of weather and is routinely used by the National Weather Service and other forecasting services. The model is based on the Navier Stokes equations, which are solved numerically on a three-dimensional grid. The model simulates four basic atmospheric properties: wind, pressure, temperature, and atmospheric water vapor. All others variables are derived from these. The standard version of WRF does not produce optical turbulence parameters. However, in this application the model was modified to make simulations of C_n^2 based on changes to the Mellor-Yamada-Janjic (MYJ) TKE scheme to diagnose the turbulent Prandtl number as a function of the Richardson number [3].

For this study WRF is configured using a nested grid system (Figure 1). The grid structure consists of an outer domain run at 9km resolution centered on the central Tropical Pacific Ocean, a regional 3km grid centered on

the Hawaiian islands, an inner 1km grid centered on the island of Maui and neighboring islands, and an ultra high resolution grid centered on the summit of Haleakala which is run at 333 meters resolution. The resolution of the vertical levels is approximately 50-100 m below 2 km above ground level (AGL), 150-250 m for 2–13 km AGL, and 500 m up to the model top (50 millibars). Numerical simulations are first initialized at 1200 UTC directly from the 0.25° Global Forecasting System (GFS) analysis produced by the National Weather Service. In our study, WRF produces a 48 hour forecast using lateral boundary conditions that are provided out to 48 hours by three-hourly GFS forecasts. After this initial "cold-start" run, WRF is run using the WRF Data Assimilation (WRFDA) system. WRFDA is used to combine the output of the previous WRF run with meteorological observations that are not routinely used in standard WRF runs to produce and improved initialization field for the next model run. Using this procedure, each subsequent run (performed every 24 hours) uses the 24 hour forecast from the previous WRF simulation to provide a first-guess of the atmospheric state. This eliminates the need to spin-up the mass and momentum fields every 24 hours. In so doing, the model has already "warmed up" and therefore essentially continues its simulation but with new assimilated data and lateral boundary conditions (Figure 2).

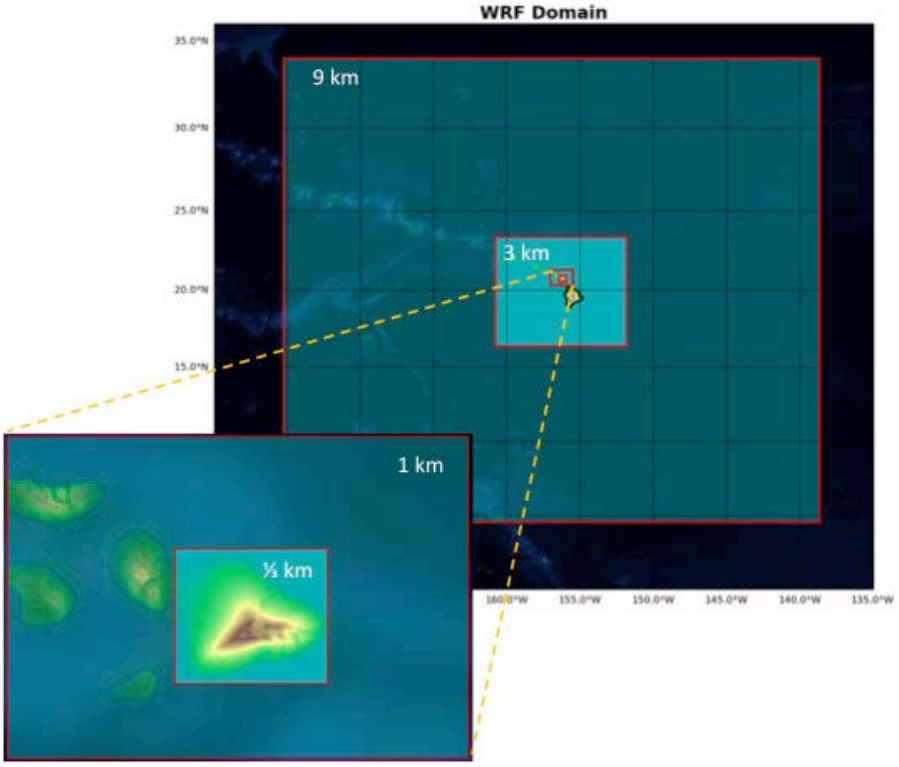

Figure 1. WRF nested grid setup featuring an ultra-high resolution grid centered on the summit of Haleakala.

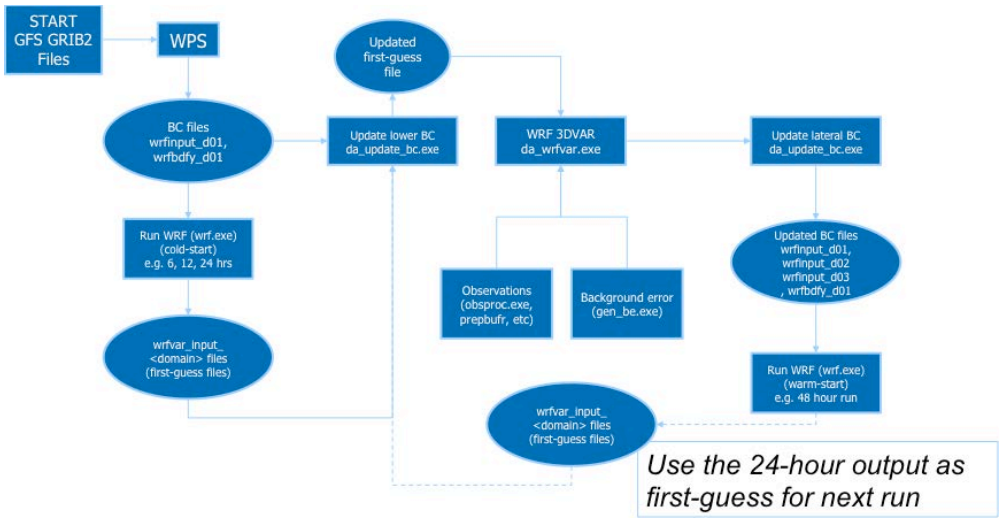

Figure 2. Flow chart showing the WRFDA and warm start system.

The WRF output files contain time-varying (up to 15 minutes), three-dimensional atmospheric variables, with values at each grid point representing standard meteorological quantities of temperature, pressure, winds, and moisture. In addition a cloud fraction parameter derived from the microphysics scheme is also generated and used to compare with our satellite-derived cloud products (see next section).

b. Satellite Products

Validation of the WRF cloud product is performed by comparing it to satellite derived clouds. Northrop Grumman has been collecting and processing multispectral satellite cloud imagery in support of FSOC atmospheric mitigation studies for more than 20 years. For this investigation, the detection of clouds from satellite imagery is performed using the Cloud Mask Generator (CMG). The CMG ingests Geostationary Operational Environmental Satellite (GOES) multispectral imagery (at 4 km, 15 minute resolution) and applies a series of single- and multi-spectral tests to detect clouds [4,5]. The GOES imager has 5 bands: visible (0.6 µm), shortwave infrared (3.9 µm) (SWIR), water vapor (6.7 µm), longwave infrared (10.7 µm) (LWIR), and split window (11.2 µm). The water vapor channel is not used for cloud detection and is replaced by a fog product at night and a shortwave reflectivity product during the day. The CMG generates a cloud/no cloud decision for every pixel by computing the difference between the LWIR temperature, visible albedo, derived products, and the dynamically computed clear sky background (CSB) each time a new GOES image is available. The classification of a pixel as clear or cloudy is based on where the calculated difference falls with respect to the threshold confidence range. Threshold confidence ranges for each test are spatially and temporally defined. The limit of the CMG cloud detection is estimated to be between 1.0 and 1.5 dB [4].

3. EXAMPLE MODEL OUTPUT

The WRF model produces dozens of atmospheric products. However, in this study we are most interested in those products directly related to making decisions about using a ground site for optical communications. Figure 3 shows the mean sea-level pressure at 9km resolution on the WRF outer grid. Centered over the central Pacific Ocean, this grid is required to fully simulate the meteorology over the summit out to 48 hours.

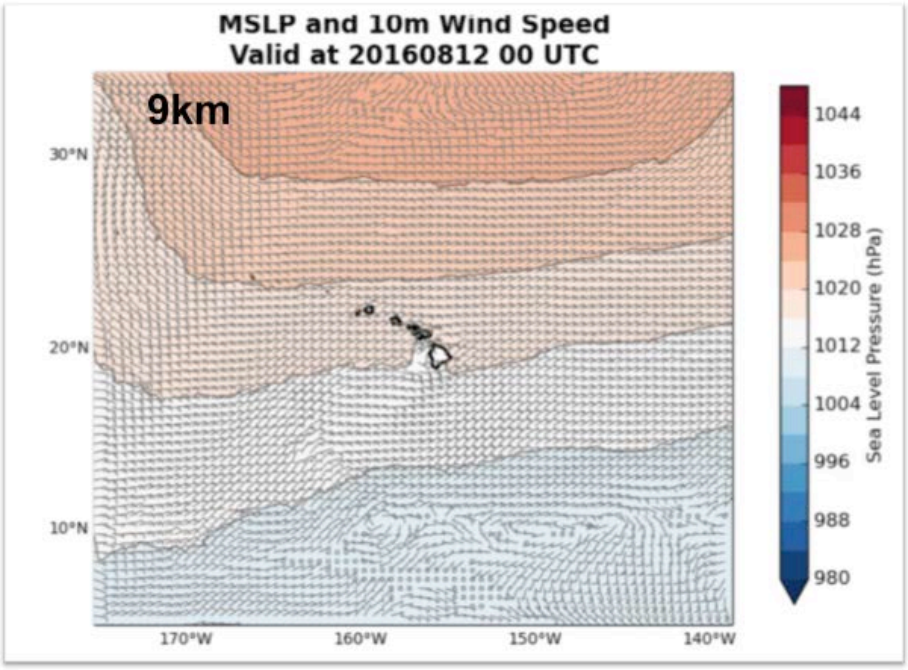

Figure 3a. WRF 9km grid of mean sea-level pressure centered over the Pacific Ocean.

Figure 3b shows the total precipitable water (TWP) of the 3km grid over the Hawaiian Islands. The TWP product is a measure of the total amount of water vapor in the atmosphere if it completely rained out, and can give some indication of the probability of clouds. Typical values range from close to zero to more than 60 millimeters. In Figure 3b, darker shades of green indicate where the TWP is highest and lighter shades of green indicate lower values of TWP. One expects the 3000 meter plus summits of Hawaii to have much less TWP given their altitude. Indeed this is the case in this simulation, particularly at Mauna Loa and Mauna Kea on the Big Island.

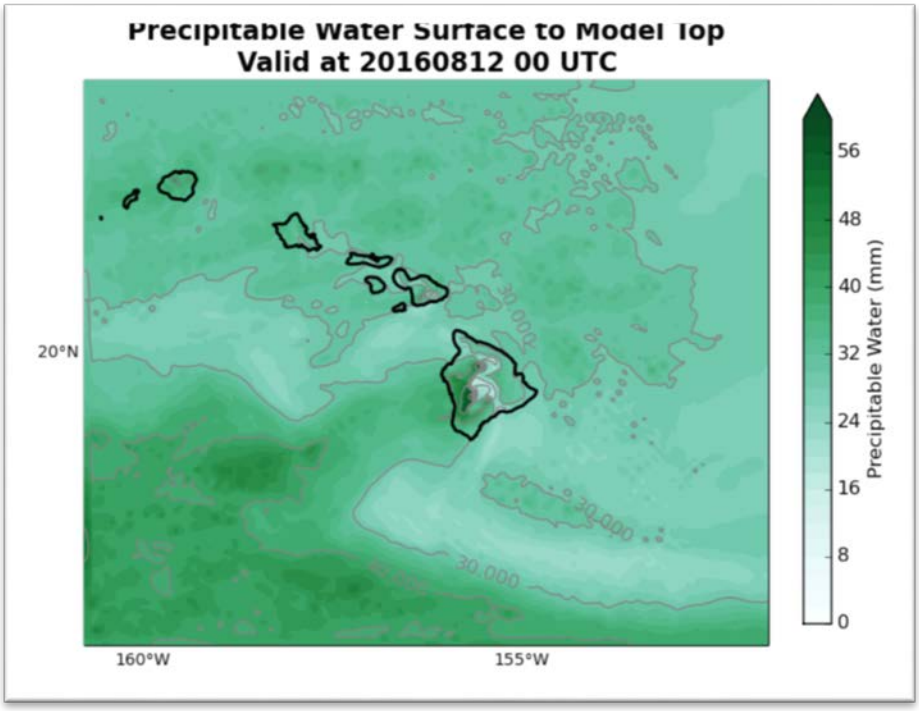

Figure 3b. Total precipitable water of the WRF 3km grid over the Hawaiian Islands.

In addition to the standard meteorological quantities, WRF is used to make three-dimensional OT simulations over this region. Our modified version of WRF computes the atmospheric refractive index structure function, C_n^2, for every three-dimensional grid point in the domain. Profiles of C_n^2 can be extracted for any line-of-sight within the domain. C_n^2 is integrated vertically to compute the Fried coherence length, r_0, which is a measure of phase distortion of an optical wave front by turbulence. This parameter represents the integrated effect of turbulence along a line of sight, and can vary rapidly over time and from one point of the sky to another. Larger values of r_0 are indicative of less turbulence and better seeing, while smaller values of r_0 represent stronger turbulence and worse seeing. The coherence length [6] is calculated by integrating C_n^2 along a path, *z*:

$$r_o = \left[0.423 \left(\frac{2\pi}{\lambda} \right)^2 \int_0^\infty C_n^2(z)\, dz \right]^{-3/5}$$

A depiction of r_0 for the inner grid, obtained by vertically integrating C_n^2, is shown in Figure 3c. Values are represented in centimeters and referenced to 1550 nanometers (nm). Warmer shades (red) indicate where r_0 values are large and thus OT is quite benign. These are typically and not surprisingly observed at higher elevations close to the summit where values can exceed 100 cm during the daytime. However, closer to sea-level, the WRF simulations show that OT is much stronger as is expected when integrating through the entire depth of the atmosphere. In previous studies [1] we have shown that WRF simulations of r_0 agree very well with observations made at the summit of Haleakala [7]. In fact WRF simulations of r_0 indicate that the summit of Haleakala has quite favorable seeing conditions relative to points at sea-level.

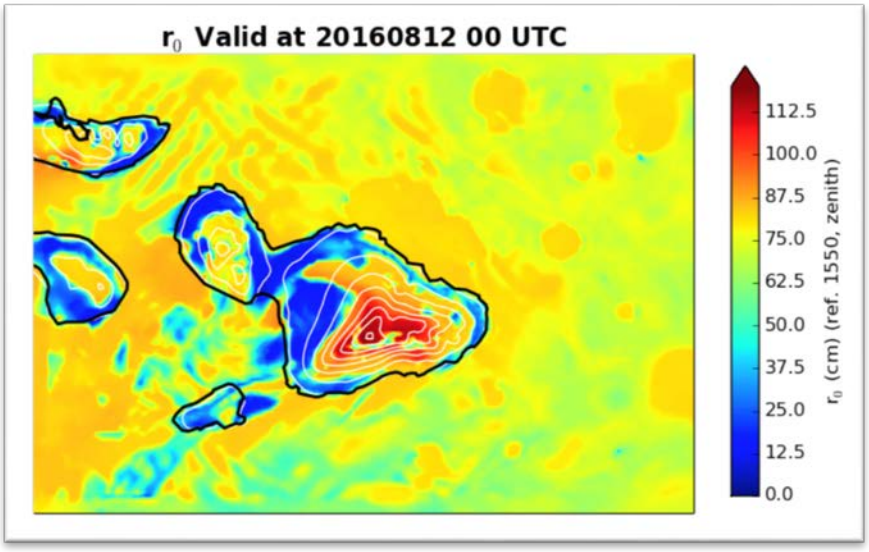

Figure 3c. Numerical simulations of r_0 derived from the surface to the top of the atmosphere. Filled contours show the values of r_0. Elevation contours are shown by the gray contour lines..

The goal of this project is to improve the forecasts of clouds using data assimilation and high resolution modeling. An ultra-high resolution inner grid run at 333 meters is run to attempt to better resolve the local meteorology of the summit. A three-dimensional example of a WRF cloud forecast for the 333 meter domain is shown in Figure 3d. For reference the 2 meter surface temperature is also shown along with streamlines of the surface winds. To orient the reader, the 3D visualization is looking North to South at Maui with Haleakala in the middle. The north coast of Maui is at the bottom of the figure and the west coast of Maui is located on the right side of the figure. This figure shows the 3D nature of the clouds that the model is simulating with data assimilation. In this case, the model is producing clouds around 1400 Local time (LT) at several areas around the mountain but below summit. The surface wind flow shows very detailed circulations that would not be resolved with coarser scale simulations. The surface temperature fields show that temperature decreases from close to 30 Celsius (C) at sea-level to approximately 6 C at the summit.

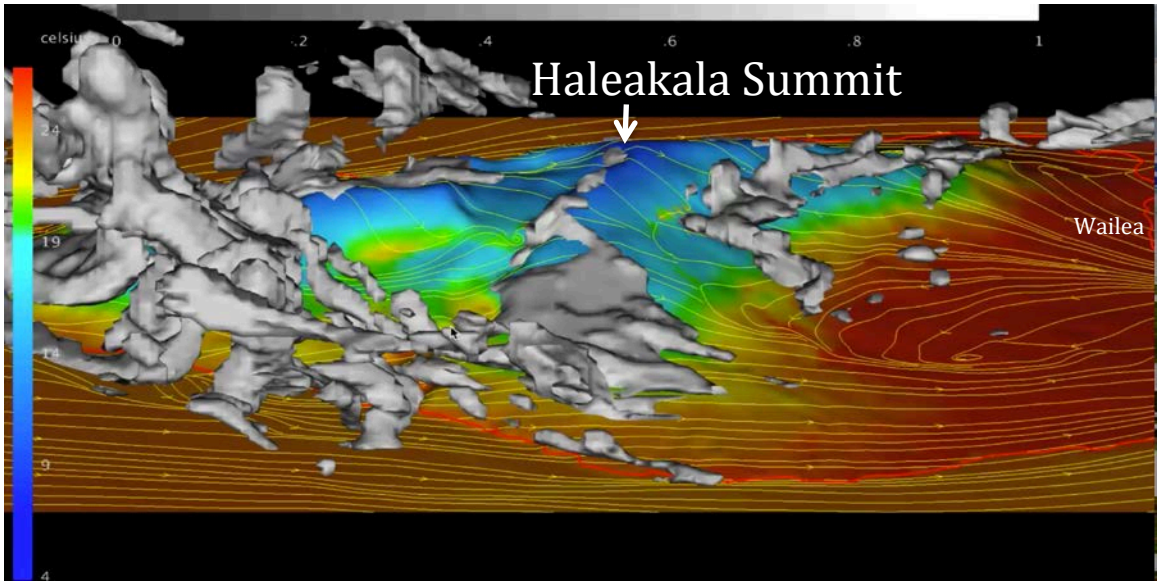

Figure 3d shows a 3D 36 hour forecast of clouds, surface temperature and winds over Maui valid at 1400 LT.

To facilitate the interpretation of the 48 hour forecast at summit, we developed a meteogram that shows relevant model output from the 333 meter resolution WRF grid. A meteogram is a convenient way to quickly assess the forecast of meteorological conditions and likelihood of clouds for a location. An example meteogram, with the time-varying forecasts of several atmospheric parameters, is shown in Figure 3e. The top plot shows the time-varying forecast of humidity, winds, and temperature as a function of height (expressed in pressure) above the summit with the freezing line indicated by the dashed black line. Plot two shows the forecast of surface wind speed and direction. Plot three shows the forecast surface temperature and dewpoint temperature. Plots four and five show the forecast of clouds and cloud heights. Plot six shows the forecast total rainfall, and plot seven shows the forecast of the trade wind inversion height and whether it is forecast to breach the summit. Finally, the bottom plot shows the 2 meter forecast humidity.

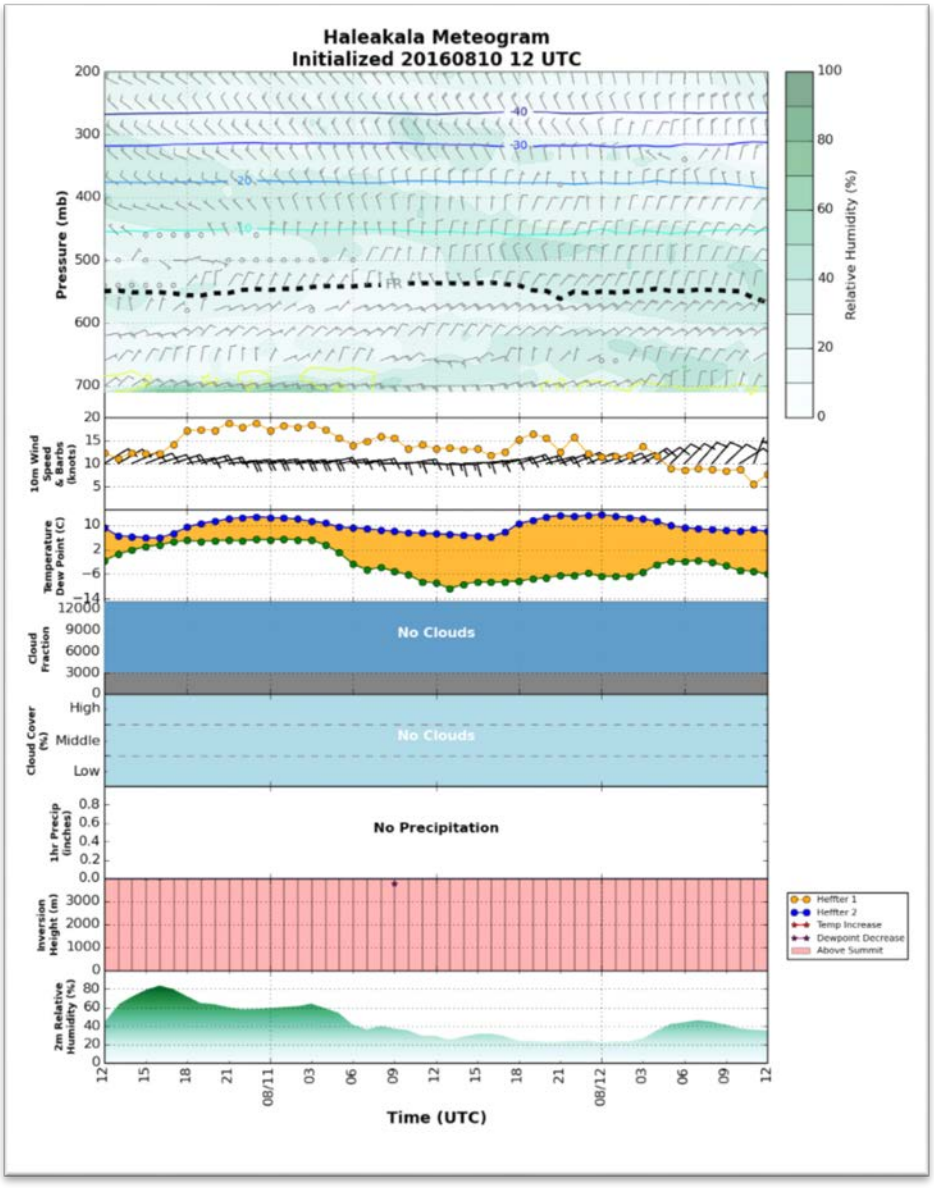

Figure 3e shows a meteogram of forecast conditions at the Haleakala summit from a 48 hour forecast of the 333 meter WRF domain. In this case the summit is forecast to be clear throughout the simulation.

4. MODEL RESULTS

WRF simulations were made for a several month period between January and May 2016 using the 1000 m and 333 m inner grids. The main purpose of this study is to: 1) estimate the value in simulating clouds at 333m versus 1000m and, 2) to compare the output to some measure of truth. Figure 4 shows the 36 hour mean cloud fraction forecast by the WRF modeling system averaged over the five month period at a) 1000 meter horizontal resolution and b) 333 m horizontal resolution. Terrain contours are overlaid to facilitate reference to the summit. Figure 4a shows the mean cloud amount for Maui at 1400 LT (daytime), with clouds ringing the mountain below the summit and relatively cloud-free conditions near summit and at sea-level. Figure 4b on the right shows the same forecast but for the 333 meter resolution inner grid. At first inspection, the results look very similar; however, upon closer inspection, small-scale details in the cloud fields can be seen near the Haleakala crater as well as in and near the many gulches on the Southeast flank of the island. These small changes, apparent in the long term averages, are even more important on a time by time basis as the 333m grids are able to better resolve summit and crater dynamics that modulate the trade wind boundary and thus clouds.

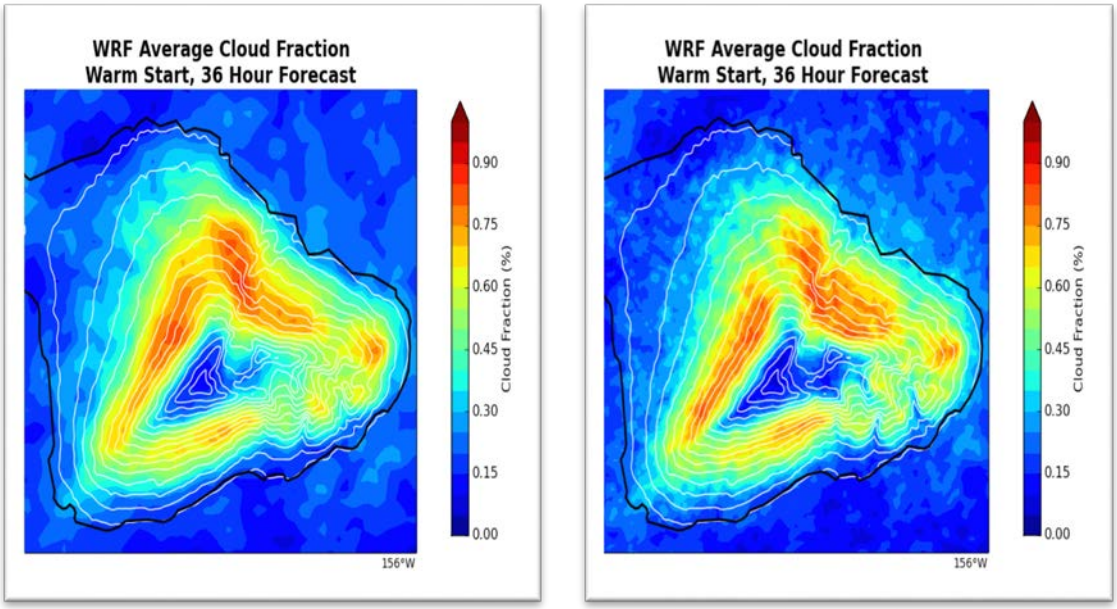

Figure 4. Mean cloud fraction derived from the 36 hour WRF cloud forecast over a five month period at a) 1000 meter resolution (left) and b) 333 meter resolution (right).

Validation of the WRF 1 km grid cloud forecasts were made by comparing them to the 1km CMG output as described in Section 2. The average cloud amount from the CMG valid at 1400 LT is shown in the top plot in Figure 5. The typical pattern of clouds around Haleakala at 1400 LT is apparent in the satellite-derived climatology (CMG), with clouds surrounding Haleakala at this time of day. Several small scale features like the Makena cloud show up in this five month average. The Makena cloud develops downwind of Haleakala each morning and is forced offshore of Makena on the Southwest side of Maui. The WRF model was initialized each day at 0200 LT and a 48 hour forecast was generated. The average cloud fraction for the 12 and 36 hour WRF forecasts (valid at 1400 LT) was computed from all the data and is shown in the bottom two plots in Figure 5. They show a remarkably similar

pattern to the CMG climatology at this time. Both the 12 and 36 hour forecasts show clouds surrounding the summit with a minimum in cloud fraction near the summit as well as the Makena cloud downwind of Haleakala. Although the magnitude of cloud fraction does not match up one for one, the general patterns are very similar.

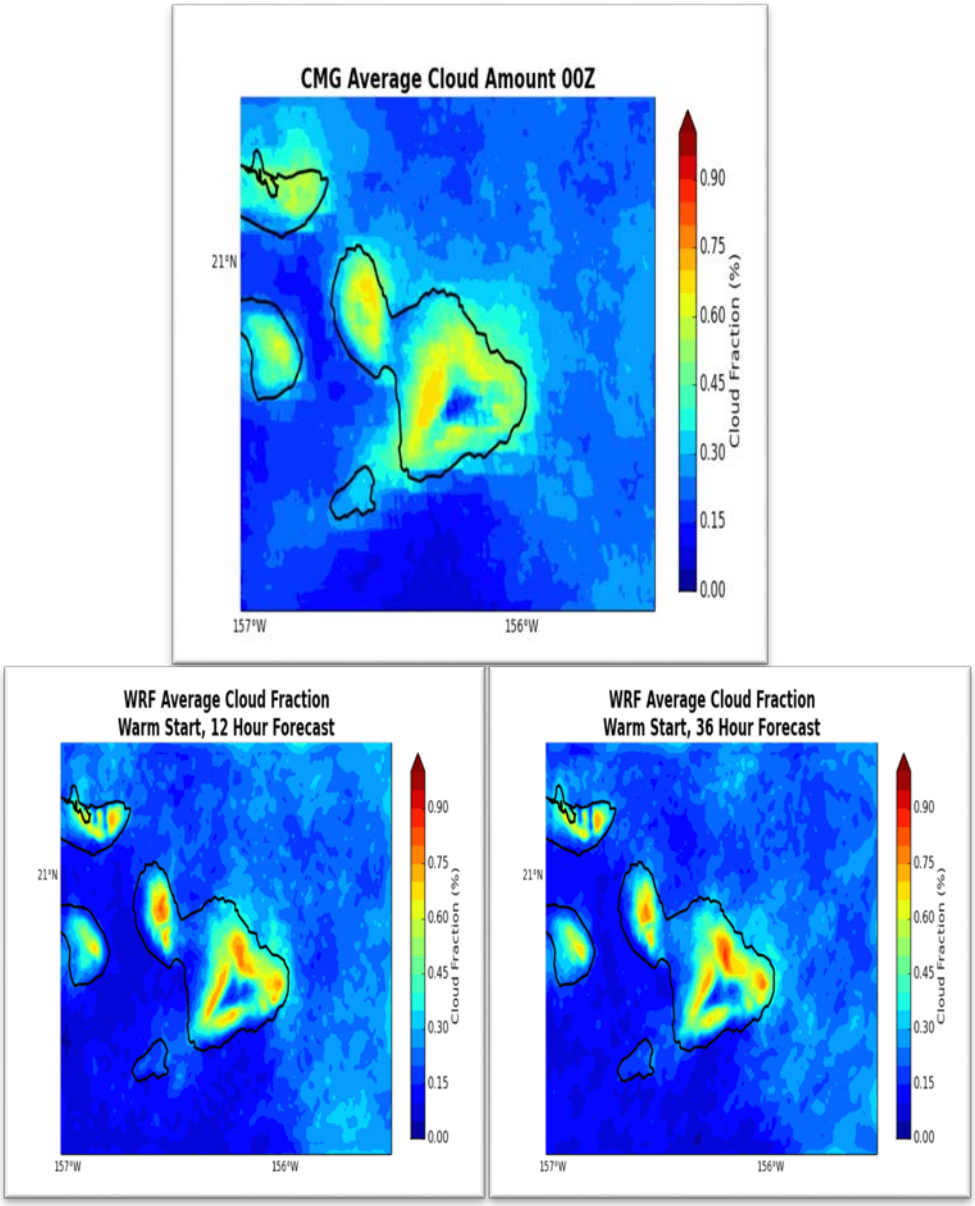

Figure 5. Mean 1km CMG cloud fraction at 1400 LT based on January - May 2016 GOES imagery (top). 1km resolution WRF 12 hour (left) and 36 hour (right) forecasts of cloud fraction valid at 1400 LT.

Evaluations of the WRF forecasts were made on a time by time basis at the top of each hour. The percentage of the time WRF correctly forecast clear and cloudy conditions as well as the percentage of false alarms and missed clouds were computed over the five month period. Figure 6 shows these results for both the summit of Haleakala

and at the airport in Kahului. Comparisons were made to the CMG output for the same time. Results indicate the forecast does not suffer as a function of forecast length; rather the forecasts have more a diurnal variation in accuracy. WRF's ability to forecast both clear and cloudy conditions routinely exceeds 70-90% at summit but is lower at sea-level. False alarms and missed clouds occur 10-30% of the time.

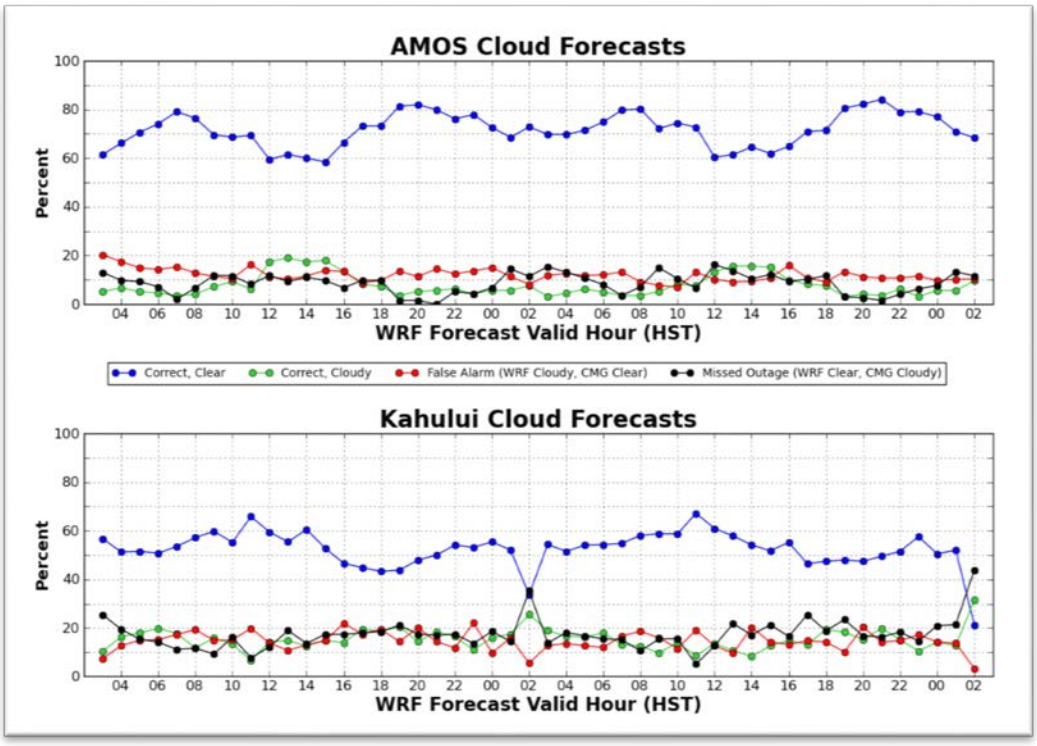

Figure 6. Percent correct clear and cloudy, and false alarms and missed clouds as a function of forecast length for a) Haleakala summit and b) Kahului.

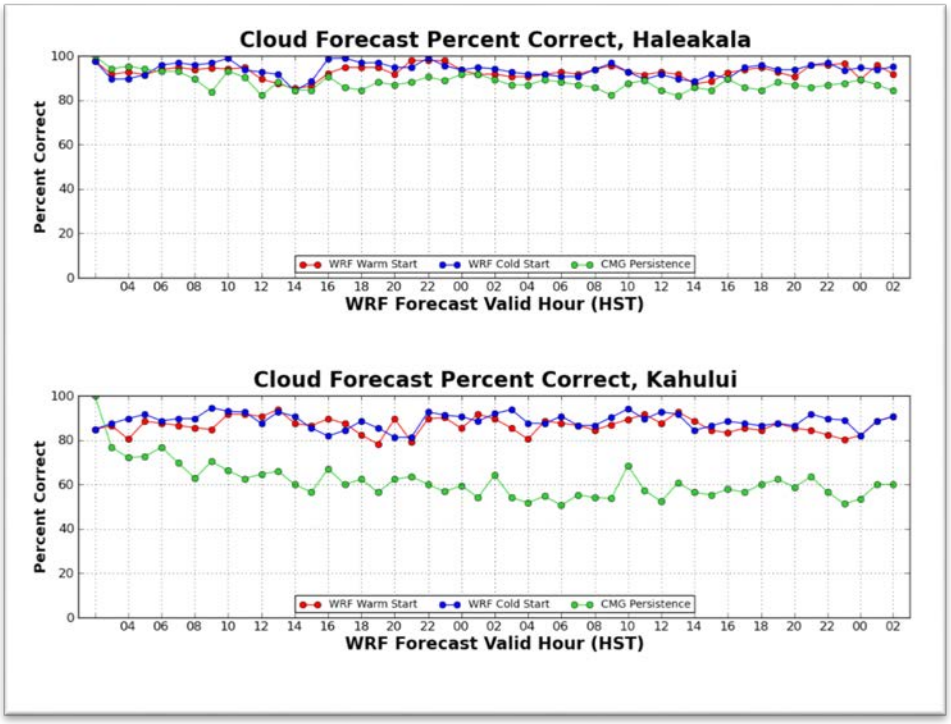

Figure 7. WRF derived forecasts (red/blue) relative to a CMG derived persistence (green) forecast for (top) Haleakala summit and (bottom) Kahului.

Figure 7 shows how the WRF forecasts compare to a measure of persistence. A persistence forecast predicts the same condition based on the current condition (i.e., it predicts no change). WRF forecasts routinely exceed a persistence forecast at both summit and sea-level. The ability to outperform persistence at summit is significant since the summit is typically cloud free and therefore there is typically no change in cloud condition. At sea-level the out performance is even greater where cloud occurrence is much larger and more variable. At these locations a persistence forecast has much less value.

5. SUMMARY AND CONCLUSIONS

This study has shown the advantage of using data assimilation and high resolution numerical modeling to improve and optimize cloud forecasts. Future work will expand upon this capability to improve initial conditions even further through direct satellite radiance assimilation.

References

[1] Alliss, R.J and B.D. Felton, 2009: "Validation of Optical Turbulence Simulations from a Numerical Weather Prediction Model in Support of Adaptive Optics Design", *Advance Maui Optical and Space Surveillance Technologies Conference*, Vol 1, p. 54.

[2] Skamarock, W. C., J. B. Klemp, J. Dudhia, D. O. Gill, D. M. Barker, M. G. Duda, X.-Y. Huang, W. Wang, and J. G. Powers, 2008: A description of the advanced research WRF version 3. NCAR Technical Note, NCAR/TN-475+STR, 113 pp.

[3] Alliss, R.J and B.D. Felton, 2014: " Numerical Simulations of Optical Turbulence Using an Advanced Atmospheric Prediction Model: Implications for Adaptive Optics Design", *Advance Maui Optical and Space Surveillance Technologies Conference*.

[4] Alliss, R.J., M. E. Loftus, D. Apling, and J. Lefever, "The Development of Cloud Retrieval Algorithms Applied to GOES Digital Data," in *10th Conference on Satellite Meteorology and Oceanography*, pp. 330–333, American Meteorological Soc., January 2000.

[5] Wojcik, G., R.J., Alliss and M.E., Craddock, "Deep Space to Ground Laser Communications in a Cloudy World", *IEEE Photonics*, Aug 2005.

[6] Fried, D. L., 1965: Statistics of a geometric representation of wavefront distortion. *J. Opt. Soc. Amer.*, **55**, 1427–1435.

[7] Bradley, E.S., L.C. Roberts, L. W. Bradford, M. Skinner, D.A. Nahrstedt, M.F. Waterson and J.R. Kuhn, 2006: Characterization of Meteorological and Seeing Conditions at Haleakala. *Publications of the Astronomical Soc. of the Pacific*, **118:**172-182.